

Measurement of the ratio of the lepton widths $\Gamma_{ee}/\Gamma_{\mu\mu}$ for the J/ψ meson

V. M. Aulchenko^{a,b}, E. M. Baldin^{a,b,*}, A. K. Barladyan^a, A. Yu. Barnyakov^a, M. Yu. Barnyakov^a, S. E. Baru^a, I. Yu. Basok^a, A. M. Batrakov^a, A. E. Blinov^a, V. E. Blinov^{a,c}, A. V. Bobrov^{a,b}, V. S. Bobrovnikov^a, A. V. Bogomyagkov^{a,b}, A. E. Bondar^{a,b}, A. R. Buzykaev^a, S. I. Eidelman^{a,b}, D. N. Grigoriev^{a,b,c}, V. R. Groshev^a, Yu. M. Glukhovchenko^a, V. V. Gulevich^a, D. V. Gusev^a, S. E. Karnaev^a, G. V. Karpov^a, S. V. Karpov^a, T. A. Kharlamova^a, V. A. Kiselev^a, V. V. Kolmogorov^a, S. A. Kononov^{a,b}, K. Yu. Kotov^a, E. A. Kravchenko^{a,b}, V. N. Kudryavtsev^a, V. F. Kulikov^{a,b}, G. Ya. Kurkin^{a,c}, E. A. Kuper^{a,b}, I. A. Kuyanov^a, E. B. Levichev^{a,c}, D. A. Maksimov^{a,b}, V. M. Malyshev^a, A. L. Maslennikov^a, O. I. Meshkov^{a,b}, S. I. Mishnev^a, I. I. Morozov^{a,b}, N. Yu. Muchnoi^{a,b}, V. V. Neufeld^a, S. A. Nikitin^a, I. B. Nikolaev^{a,b}, I. N. Okunev^a, A. P. Onuchin^{a,c}, S. B. Oreshkin^a, I. O. Orlov^{a,b}, A. A. Osipov^a, I. V. Ovtin^{a,c}, S. V. Peleganchuk^a, S. G. Pivovarov^{a,c}, P. A. Piminov^a, V. V. Petrov^a, A. O. Poluektov^a, V. G. Prisekin^a, O. L. Rezanova^{a,b}, A. A. Ruban^a, V. K. Sandyrev^a, G. A. Savinov^a, A. G. Shamov^a, D. N. Shatilov^a, B. A. Shwartz^{a,b}, E. A. Simonov^a, S. V. Sinyatkin^a, A. N. Skrinsky^a, A. V. Sokolov^{a,b}, A. M. Sukharev^a, E. V. Starostina^{a,b}, A. A. Talyshev^{a,b}, V. A. Tayursky^a, V. I. Telnov^{a,b}, Yu. A. Tikhonov^{a,b}, K. Yu. Todyshev^{a,b}, G. M. Tumaikin^a, Yu. V. Usov^a, A. I. Vorobiov^a, V. N. Zhilich^a, V. V. Zhulanov^{a,b}, A. N. Zhuravlev^{a,b}

^a*Budker Institute of Nuclear Physics, 11, akademika Lavrentieva prospect, Novosibirsk, 630090, Russia*

^b*Novosibirsk State University, 2, Pirogova street, Novosibirsk, 630090, Russia*

^c*Novosibirsk State Technical University, 20, Karl Marx prospect, Novosibirsk, 630092, Russia*

Abstract

The ratio of the electron and muon widths of the J/ψ meson has been measured using direct J/ψ decays in the KEDR experiment at the VEPP-4M electron-positron collider. The result

$$\Gamma_{e^+e^-}(J/\psi)/\Gamma_{\mu^+\mu^-}(J/\psi) = 1.0022 \pm 0.0044 \pm 0.0048 \text{ (0.65\%)}$$

is in good agreement with the lepton universality. The experience collected during this analysis will be used for J/ψ lepton width determination with up to 1% accuracy.

Keywords: J/ψ meson, lepton width, lepton universality

PACS: 13.20.Gd, 13.66.De, 14.40.Gx

1. Introduction

The lepton width of a hadronic resonance $\Gamma_{\ell\ell}$ describes fundamental properties of the strong interaction potential [1]. Comparison of the electron and muon widths $\Gamma_{ee}/\Gamma_{\mu\mu}$ allows one to test the lepton universality and provides information on the models predicting new forces differentiating between lepton species [2].

Currently the two most precise values of the ratio of the J/ψ meson lepton widths come from the CLEO results obtained in 2005 [3] and the recent BESIII measurement [4]. For that analysis both experiments used the $\psi(2S) \rightarrow J/\psi\pi^+\pi^-$, $J/\psi \rightarrow \ell^+\ell^-$ decay chain ($\ell = e, \mu$).

Our analysis is based on direct J/ψ decays. Its scheme and the sources of systematic uncertainties are completely different from those in the CLEO and BESIII measurements. This analysis continues the work on the lepton width determination [5] but uses an independent statistical sample. In the future we anticipate precise measurement of the J/ψ lepton width at the 1% level.

A large resonance cross section provides high statistics of J/ψ decays even with a relatively low collider luminosity. The integrated luminosity collected off resonance gives information about the QED continuum background. In addition to subtracting the QED background for calculating the numbers of the $J/\psi \rightarrow \ell^+\ell^-$ decays, one has to suppress cosmic ray events, J/ψ hadronic decays and take into account the interference between the resonance $J/\psi \rightarrow \ell^+\ell^-$ process and QED background. The QED backgrounds for the $J/\psi \rightarrow e^+e^-$ and $J/\psi \rightarrow \mu^+\mu^-$ processes are fundamentally different due to Bhabha scattering.

2. Experiment

The experiment was performed with the KEDR detector [6] at the VEPP-4M e^+e^- collider [7]. An integrated luminosity of 2.1 pb^{-1} corresponding to production of about $6.5 \cdot 10^6$ J/ψ mesons was collected in the J/ψ resonance energy range from 3086 to 3107 MeV. The experimental data sample was divided into two parts (Fig. 1 and Fig. 2 for e^+e^- and $\mu^+\mu^-$ events, respectively): “on-resonance”, with $|W - M_{J/\psi}| < 1.3 \text{ MeV}$ ($\approx 80\%$ of statistics), and “off-resonance”, with $|W - M_{J/\psi}| >$

*Corresponding author, e-mail: E.M.Baldin@inp.nsk.su

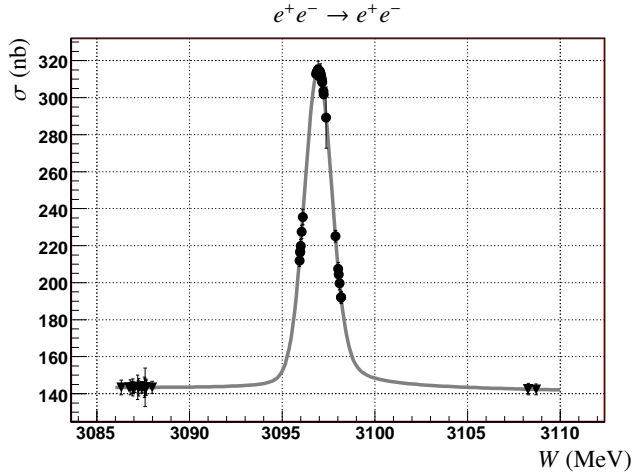


Figure 1: e^+e^- cross section expected from the experimental runs; dots: “on-resonance” data, triangles: “off-resonance” data. The curve is the theoretical di-electron cross section (1) in the experimental energy and angle ranges.

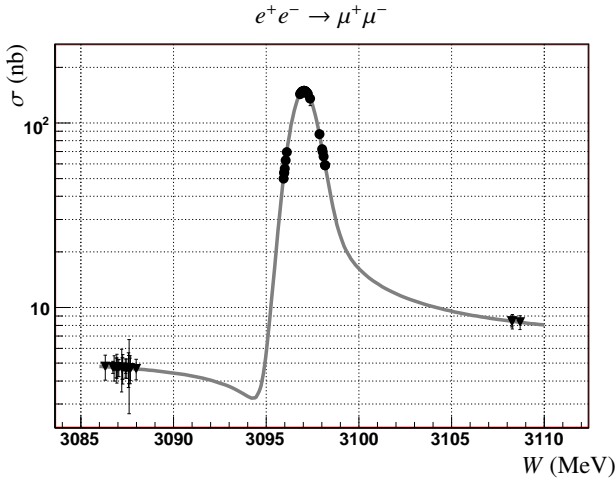


Figure 2: $\mu^+\mu^-$ cross section expected from the experimental runs; dots: “on-resonance” data, triangles: “off-resonance” data. The curve is the theoretical dimuon cross section (2) in the experimental energy and angle ranges.

8.9 MeV, where W is the center-of-mass energy. The energy spread σ_W was about 0.7 MeV.

KEDR is a general-purpose detector with solenoidal magnetic field. It consists of a vertex detector, a drift chamber, scintillation time-of-flight counters, aerogel Cherenkov counters, a barrel liquid krypton calorimeter, an endcap CsI calorimeter, and a muon system built in the yoke of a superconducting coil generating a field of 0.65 T. The detector also includes a tagging system to detect scattered electrons for a study of two-photon processes. The on-line luminosity is measured by two independent single bremsstrahlung monitors.

The VEPP-4M collider can operate in the wide range of beam energy from 1 to 6 GeV. The peak luminosity in the J/ψ energy region is about $2 \times 10^{30} \text{ cm}^{-2}\text{s}^{-1}$. One of the main features of the VEPP-4M is its capability to precisely measure the beam energy using two techniques [8]: resonant depolarization and infrared light Compton backscattering.

3. Theory

In the soft photon approximation, analytical expressions for the $e^+e^- \rightarrow \ell^+\ell^-$ cross sections near a narrow resonance including radiative corrections are presented in Eqs. (1) and (2) below:

$$\left(\frac{d\sigma}{d\Omega}\right)_{\text{th.}}^{ee \rightarrow ee} = \frac{1}{M^2} (1 + \delta_{\text{rc}}) \left\{ \frac{9}{4} \frac{\Gamma_{e^+e^-}^2}{\Gamma M} (1 + \cos^2 \theta) \text{Im} \mathcal{F} - \frac{3\alpha}{2} \frac{\Gamma_{e^+e^-}}{M} \left[(1 + \cos^2 \theta) - \frac{(1 + \cos \theta)^2}{(1 - \cos \theta)} \right] \text{Re} \mathcal{F} \right\} + \left(\frac{d\sigma}{d\Omega}\right)_{\text{QED}}^{ee}, \quad (1)$$

$$\left(\frac{d\sigma}{d\Omega}\right)_{\text{th.}}^{ee \rightarrow \mu\mu} = \frac{1}{M^2} (1 + \delta_{\text{rc}}) \left\{ \frac{9}{4} \frac{\Gamma_{e^+e^-} \Gamma_{\mu^+\mu^-}}{\Gamma M} \text{Im} \mathcal{F} - \frac{3\alpha}{2} \frac{\sqrt{\Gamma_{e^+e^-} \Gamma_{\mu^+\mu^-}}}{M} \text{Re} \mathcal{F} \right\} (1 + \cos^2 \theta) + \left(\frac{d\sigma}{d\Omega}\right)_{\text{QED}}^{\mu\mu}, \quad (2)$$

$$\mathcal{F} = \frac{\pi\beta}{\sin(\pi\beta)} \left(\frac{\frac{M}{2}}{-W + M - \frac{i\Gamma}{2}} \right)^{1-\beta}, \quad \beta = \frac{4\alpha}{\pi} \left(\ln \frac{W}{m_e} - \frac{1}{2} \right) \approx 0.077,$$

$$\delta_{\text{rc}} = \frac{3}{4}\beta + \frac{\alpha}{\pi} \left(\frac{\pi^2}{3} - \frac{1}{2} \right) + \beta^2 \left(\frac{37}{96} - \frac{\pi^2}{12} - \frac{\ln(W/m_e)}{36} \right),$$

where W is the center-of-mass energy, and θ is the lepton scattering angle with respect to the electron beam direction. Corrections to the vacuum polarization in the interference terms have been omitted.

The formulae used in this analysis are based on the analytical expression for the radiative correction integral in the soft photon approximation (SPA), first obtained in [9]. The accuracy was improved using [10] as described in [11].

To compare experimental data with the theoretical cross sections, it is necessary to perform their convolution with a distribution of the total beam energy, which is assumed to be Gaussian:

$$\sigma^{\ell\ell}(W) = \int \frac{1}{\sqrt{2\pi}\sigma_W} \exp\left(-\frac{(W - W')^2}{2\sigma_W^2}\right) \sigma_{\text{th.}}^{\ell\ell}(W') dW'. \quad (3)$$

The beam energy spread σ_W is much larger than the J/ψ full width Γ .

4. Event selection

The following selection requirements were imposed on both e^+e^- and $\mu^+\mu^-$ events (the + and - superscripts correspond to a positive particle and negative one, respectively):

1. two charged tracks with opposite signs from a common vertex in the interaction region,
2. the total energy deposition in the calorimeter (outside the two energy clusters belonging to the selected particles) is < 0.15 GeV,
3. polar θ and azimuthal φ acollinearity $< 10^\circ$,
4. the momentum $p^\pm > 0.5$ GeV.

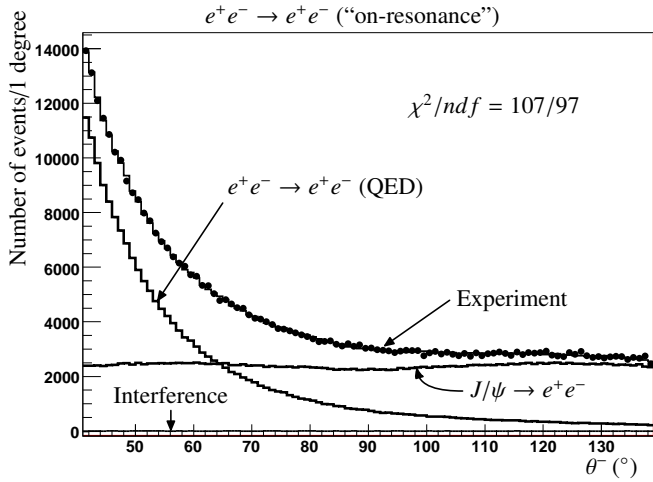


Figure 3: Distribution of the electron scattering angle for selected $e^+e^- \rightarrow e^+e^-$ events in the “on-resonance” data part. The dots represent the experiment. The labeled histograms represent the simulation: Bhabha (QED), $J/\psi \rightarrow e^+e^-$ decays and interference term. The histogram corresponding to the sum of the three contributions is under the experimental dots.

Only for the e^+e^- selection: the energy deposition for each particle $E^\pm > 0.7 \text{ GeV}$; $\theta^- \in (41 \div 139)^\circ$ and $\theta^+ \in (38 \div 142)^\circ$. The fiducial polar angle θ is restricted by the physical edges of the liquid krypton calorimeter ($37 \div 143)^\circ$.

Only for the $\mu^+\mu^-$ selection: $0.06 \text{ GeV} < E^\pm < 0.7 \text{ GeV}$; $\theta^- \in (49 \div 131)^\circ$ and $\theta^+ \in (46 \div 134)^\circ$. The polar angle θ is restricted by the edges of the muon system. To suppress the background of cosmic events we employed the time-of-flight system. For suppression of the background from J/ψ hadronic decays, a hit in the muon system is required for a μ^- track.

The θ^- angle distributions of the selected events are shown in Fig. 3 and Fig. 4 for e^+e^- and $\mu^+\mu^-$, respectively.

5. Simulation

The contributions of the e^+e^- and $\mu^+\mu^-$ resonance and interference events were simulated according to the theoretical angular distributions (1) and (2), respectively. The final state radiation was taken into account using the PHOTOS [12] package.

For the resonance contribution of $\mu^+\mu^-$ due to the relatively high mass of muons, a more precise expression for the angular distribution $\frac{d\sigma}{d\Omega} \propto \beta \times (1 + \cos^2\theta + (1 - \beta^2) \times \sin^2\theta)$ was taken. The contribution of the $\sin^2\theta$ term to this analysis is about 0.2%.

The uncertainty in the Bhabha process simulation was evaluated via comparison of our result with two independent event generators: BHWIDE [13] and MCGPJ [14]. For the $e^+e^- \rightarrow \gamma\gamma$ process, the BABAYAGA generator [15] was employed. For estimating the J/ψ background, the BES generator [16] was used.

To take the coincidence of the signal and background into account, we added the random events recorded every $5 \cdot 10^{-5}$ beam crossing to the simulated events.

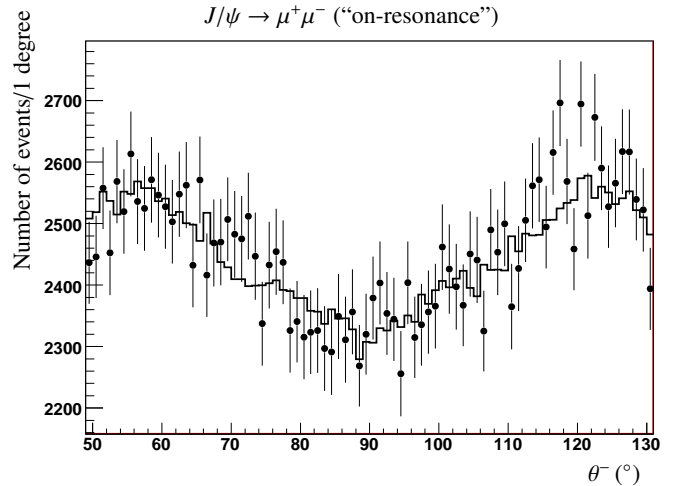


Figure 4: Distribution of the μ^- scattering angle for $J/\psi \rightarrow \mu^+\mu^-$ events in the “on-resonance” data part. The dots represent the experiment. The histogram represents the simulation.

Event number	N_{ee}	$N_{\mu\mu}$
“on-resonance”	425786 ± 658	162515 ± 406
QED (bck)	190345 ± 770	5750 ± 181
$J/\psi \rightarrow \text{hadr. (bck)}$	373	215
$J/\psi \rightarrow \ell\ell$ decays	235298 ± 774	156550 ± 447
Efficiency	$\varepsilon_{ee}, \%$	$\varepsilon_{\mu\mu}, \%$
ε_{ToF}	—	77.78
ε	60.14	51.55
$N(J/\psi \rightarrow \ell\ell)/\varepsilon$	391281 ± 1287	390412 ± 1113

Table 1: Summary of observed events, principal backgrounds, signals and their efficiency. The QED background events also include interference corrections. The efficiency ε_{ToF} corresponds to the ToF time measurement inefficiency. The stated errors are statistical only.

6. $J/\psi \rightarrow \ell^+\ell^-$ event counting

We begin our analysis by determining independently the number of e^+e^- and $\mu^+\mu^-$ events produced in J/ψ decays.

A summary of observed events, principal backgrounds, signals and their efficiency is presented in Table 1.

In Fig. 3 we show the distribution of the electron scattering angle for selected $e^+e^- \rightarrow e^+e^-$ events in the resonance data part. The displayed points represent the experimental values, while the histograms correspond to the simulation. The angular distribution of Bhabha events differs from that of $J/\psi \rightarrow e^+e^-$ decays. At small angles the Bhabha scattering prevails, while at large angles events of resonance decay dominate. So, these processes can be separated by using only a data sample collected “on-resonance”. The “off-resonance” events are not required.

The “on-resonance” data sample was collected in the vicinity of the resonance peak. Thus we have to take into account the interference effects between J/ψ decays and QED background (the histogram close to zero in Fig. 3). However, the interference effects are an $\sim 1\%$ correction only.

For separating $J/\psi \rightarrow e^+e^-$ events from the Bhabha QED background, the number of observed experimental events was

fitted to the expected contributions:

$$\frac{dN_{ee}^{\text{obs}}(\theta)}{d\theta} = n \times \text{Res}(\theta) + \langle C(E) \rangle \times \text{Int}(\theta) + L \times \text{QED}(\theta), \quad (4)$$

where n and L are the fit parameters which correspond to the number of observed $J/\psi \rightarrow e^+e^-$ events and to the absolute luminosity calibration, respectively. $\text{Res}(\theta)$, $\text{Int}(\theta)$ and $\text{QED}(\theta)$ are the angular distributions from the simulation for the resonance, interference and Bhabha QED background, respectively (sec. 5). The same histograms as presented in Fig. 3 with one degree bin width were used in the fitting procedure. Thus from the detection efficiency $\varepsilon_{J/\psi \rightarrow ee}$ we can calculate the number of J/ψ decays during the experiment: $N_{J/\psi \rightarrow ee} = n/\varepsilon_{J/\psi \rightarrow ee}$. The $\text{Res}(\theta)$, $\text{Int}(\theta)$ and $\text{QED}(\theta)$ angular distributions and this efficiency were determined from the simulation and corrected using information about performance of various detector subsystems. The statistical uncertainty of the number of e^+e^- decays is 0.33%.

The $\langle C(E) \rangle$ coefficient, which reflects the energy variation in the data set, is calculated from theory, see Eq. (1), and is determined by the interference magnitude.

The same procedure was performed for the continuum statistics, since in our “off-resonance” data, the resonant contribution and interference effects are also not completely negligible. The number of Bhabha events in continuum is necessary to calculate the number of $J/\psi \rightarrow \mu^+\mu^-$ decays.

For calculating the number of $\mu^+\mu^-$ decays (Fig. 2) we have to take the interference into account, subtract the QED background and divide that by the detection efficiency:

$$N_{J/\psi \rightarrow \mu\mu} = \frac{\left\{ N_{\text{res}}^{\text{exp}} - N_{\text{int}}^{\text{th}} - \frac{L_{\text{res}}}{L_{\text{cont}}} \times (N_{\text{cont}}^{\text{exp}} - N_{\text{int}}^{\text{th}}) \right\}}{\varepsilon_{J/\psi \rightarrow \mu\mu}}. \quad (5)$$

As in the e^+e^- case, the efficiency was determined from the simulation and corrected using information about performance of various detector subsystems. The statistical error of the number of $J/\psi \rightarrow \mu^+\mu^-$ decays is 0.29%.

7. Systematic uncertainties

A list of main systematic uncertainties in the ratio of $\Gamma_{ee}/\Gamma_{\mu\mu}$ is presented in Table 2.

Luminosity, energy measurement and theoretical radiation corrections are important mainly for the interference effects, which are small corrections only.

The J/ψ hadronic decay contribution to the selected $\mu^+\mu^-$ and e^+e^- events was estimated by the Monte Carlo method and the scale of uncertainty was estimated using the nuclear interaction simulation packages FLUKA [17] and GHEISHA [18] (as implemented in GEANT 3.21 [19]). The uncertainty of the contribution from the $e^+e^- \rightarrow \gamma\gamma$ background is negligible. A possible contribution to e^+e^- events from cosmic events was estimated using the muon and the time-of-flight systems.

From the trigger “point of view”, the main difference between e^+e^- and $\mu^+\mu^-$ events is the high energy deposition for e^+e^- events in the calorimeter. The trigger calorimeter thresholds were too high for $\mu^+\mu^-$ events, but the efficiency for e^+e^-

Source	Correct., %	Err., %
Interference		
Luminosity		0.01
Energy measurement		0.02
Radiation corrections		0.10
Background		
$J/\psi \rightarrow$ hadrons	-0.05	0.10
$e^+e^- \rightarrow \gamma\gamma$	-0.07	
Cosmic		0.07
Simulation		
Bhabha		0.11
PHOTOS	+0.20	0.02
Trigger		
1st level	-0.70	0.20
2nd level	-1.17	0.11
Event selection		
tracking system	+1.18	0.10
calorimeter	+0.27	0.10
muon system	-0.12	0.04
θ angle cuts		0.10
θ angle determination		0.14
Selection asymmetry		0.14
ToF inefficiency	-22.2	0.26
Total Systematic Uncertainties		0.48

Table 2: Summary of the systematic relative uncertainties for the ratio of $\Gamma_{ee}/\Gamma_{\mu\mu}$. The first column is the source of uncertainty, the second is the correction to the result which was applied due to this source if applicable and the third one is the uncertainty.

selected events is 99.0%. The efficiency of the calorimeter trigger for e^+e^- selected events was estimated with the help of the ToF system trigger. The first level trigger selected $\mu^+\mu^-$ events using the ToF system only, but e^+e^- events in addition to the ToF system, could be independently selected with the calorimeter.

The first level trigger $\mu^+\mu^-$ inefficiency $\approx 0.7\%$ was measured using the data from special “cosmic” runs with soft ToF system restrictions. The uncertainty $\approx 0.2\%$ was estimated by comparison of the inefficiency obtained with differently selected subsets of the cosmic events. The second level trigger $\mu^+\mu^-$ inefficiency $\approx 1.17\%$ and uncertainty $\approx 0.11\%$, mainly due to the vertex detector, were estimated using the e^+e^- data.

The corrections to the detector efficiency were obtained using experimental data. Event selection uncertainties were estimated via variations of the cuts. The uncertainty of the θ angle determination was evaluated via comparison of the angular measurements performed in the tracking system and the liquid krypton calorimeter.

The event selection was asymmetrical with respect to the particle sign. The same procedures were performed with the opposite sign. The final result is the half-sum and the estimated uncertainty is the half-difference of the results of these two procedures.

The main error comes from the ToF time measurement inefficiency due to a dead time in the time expander. It is a rather large correction as compared with the others. The time distribu-

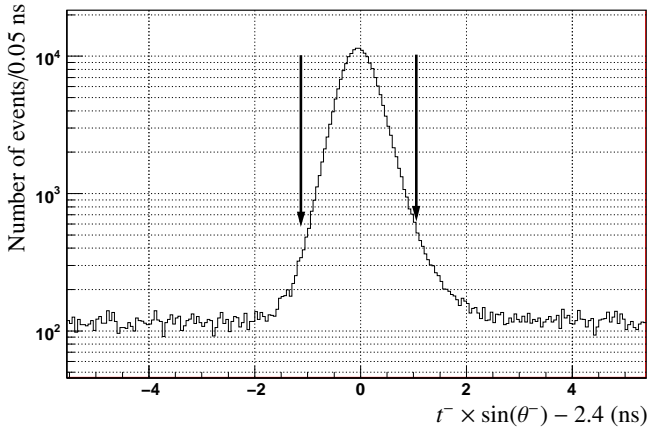


Figure 5: The ToF time distribution for μ^- . The arrows represent the ToF cuts $\pm 3\sigma_t$, where $\sigma_t = 0.36$ ns is a ToF time resolution.

tion for μ^- is presented in Fig. 5. The cosmic background is flat and could be easily measured. Thus it is possible to estimate the efficiency for the μ^+ with μ^- time cuts applied and vice versa. The net time-of-flight efficiency is a product of these values:

$$\varepsilon_{\text{ToF}} = \varepsilon_{\mu^+(\mu^-)} \times \varepsilon_{\mu^-(\mu^+)} = (77.78 \pm 0.12 \pm 0.03)\%$$

provided that there are no correlations. This assumption was checked with an electron data sample ($\varepsilon_{\text{ToF real}}^{ee} = 76.35\%$ as compared with $\varepsilon_{\text{ToF calc}}^{ee} = \varepsilon_{e^+(e^-)} \times \varepsilon_{e^-(e^+)} = 76.51\%$). The relative difference

$$\delta\varepsilon_{\text{ToF}}/\varepsilon_{\text{ToF}} = (\varepsilon_{\text{ToF real}}^{ee} - \varepsilon_{\text{ToF calc}}^{ee})/\varepsilon_{\text{ToF}}^{ee} = 0.21\%$$

estimates the possible correlation magnitude. Adding the statistical uncertainty ($\simeq 0.12\%$) and uncertainty from the cosmic background ($\simeq 0.03\%$) estimation in quadrature, we obtain a total systematic uncertainty of 0.26%.

8. Result

To conclude, a measurement of the ratio of the lepton widths Γ_{ee} and $\Gamma_{\mu\mu}$ has been performed at the VEPP-4M collider using the KEDR detector. Our final result is as follows:

$$\Gamma_{e^+e^-}(J/\psi)/\Gamma_{\mu^+\mu^-}(J/\psi) = 1.0022 \pm 0.0044 \pm 0.0048.$$

Adding the statistical and systematic errors in quadrature, we obtain a total ratio uncertainty of about 0.65%. This result is in good agreement with the lepton universality and provides information for the models predicting new forces differentiating between lepton species [2]. A comparison with other measurements is presented in Fig. 6. The experience collected during this analysis will be used for a measurement of the J/ψ lepton width at the 1% level, important for various applications, e.g., for a determination of the charm quark mass [21].

The authors are grateful to J. Kühn and M. Pospelov for fruitful discussions. This work is supported by the Ministry of Education and Science of the Russian Federation, RFBR grants 12-02-00023-a, 12-02-01076-a, 14-02-31401, Sci. School Nsh-5320.2012.2 grant and DFG grant HA 1457/9-1.

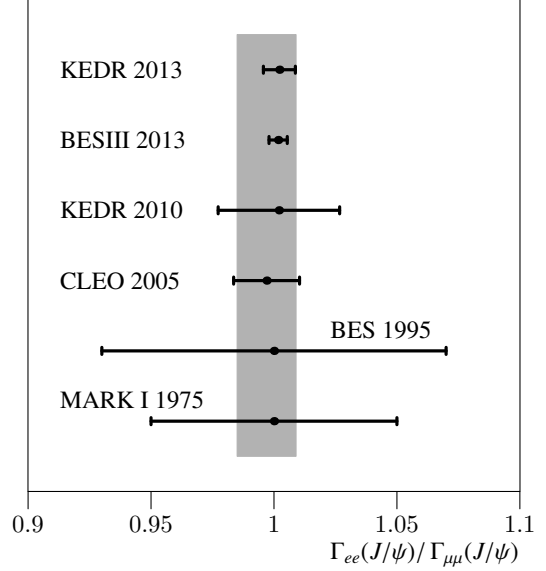


Figure 6: Comparison of the current and earlier measurements of the ratio $\Gamma_{ee}/\Gamma_{\mu\mu}$. The vertical grey band marks the average value and uncertainty of the 2012 PDG compilation [20].

References

- [1] N. Brambilla *et al.*, *Eur. Phys. J.* **C71**, 1534 (2011).
- [2] B. Batell, D. McKeen, and M. Pospelov, *Phys. Rev. Lett.* **107**, 011803 (2011), arXiv:1103.0721.
- [3] CLEO Collaboration, Z. Li *et al.*, *Phys. Rev.* **D71**, 111103 (2005), arXiv:hep-ex/0503027.
- [4] BESIII Collaboration, M. Ablikim *et al.*, *Phys. Rev.* **D88**, 032007 (2013), arXiv:1307.1189.
- [5] KEDR Collaboration, V. V. Anashin *et al.*, *Phys. Lett. B* **685**, 134 (2010), arXiv:0912.1082.
- [6] KEDR Collaboration, V. V. Anashin *et al.*, *Phys. Part. Nucl.* **44**, 657 (2013).
- [7] V. Anashin *et al.*, Stockholm 1998, EPAC 98*, 400 (1998), Prepared for 6th European Particle Accelerator Conference (EPAC 98), Stockholm, Sweden, 22-26 Jun 1998.
- [8] V. Blinov *et al.*, *Nucl. Instrum. Meth.* **A598**, 23 (2009).
- [9] Y. I. Asimov *et al.*, *JETP Lett.* **21**, 172 (1975).
- [10] E. A. Kuraev and V. S. Fadin, *Sov. J. Nucl. Phys.* **41**, 466 (1985).
- [11] KEDR Collaboration, V. V. Anashin *et al.*, *Phys. Lett.* **B711**, 292 (2012), arXiv:1109.4205.
- [12] E. Barberio and Z. Was, *Comput. Phys. Commun.* **79**, 291 (1994).
- [13] S. Jadach, W. Flączek, and B. F. L. Ward, *Phys. Lett. B* **390**, 298 (1997).
- [14] A. B. Arbuzov, G. V. Fedotovich, F. V. Ignatov, E. A. Kuraev, and A. L. Sibidanov, *Eur. Phys. J.* **C46**, 689 (2006), hep-ph/0504233.
- [15] C. Calame and C. Michel, *Phys. Lett.* **B520**, 16 (2001), arXiv:hep-ph/0103117.
- [16] J. C. Chen, G. S. Huang, X. R. Qi, D. H. Zhang, and Y. S. Zhu, *Phys. Rev.* **D62**, 034003 (2000).
- [17] G. Battistoni *et al.*, The FLUKA code: Description and benchmarking, in *Proceedings of the Hadronic Shower Simulation Workshop 2006*, edited by M. Albrow and R. Raja, AIP Conference Proceeding Vol. 896, p. 31, 2007.
- [18] H. Fesefeldt, The simulation of hadronic showers: physics and applications, 1985, PITHA-85-02, CERN-DD-EE-81-1, CERN-DD-EE-80-2.
- [19] <http://www.wasd.web.cern.ch/www.wasd/geant/>.
- [20] Particle Data Group, J. Beringer *et al.*, *Phys. Rev.* **D86**, 010001 (2012).
- [21] J. H. Kühn, M. Steinhauser, and C. Sturm, *Nucl. Phys.* **B778**, 192 (2007), arXiv:hep-ph/0702103.